Finsler Geometry on Higher Order Tensor Fields and Applications to High Angular Resolution Diffusion Imaging*

Laura Astola and Luc Florack

Department of mathematics and computer science, Eindhoven University of Technology, PO Box 513, NL-5600 MB Eindhoven, The Netherlands
l.j.astola@tue.nl

Abstract. We study three dimensional volumes of higher order tensors, using Finsler geometry. The application considered here is in medical image analysis, specifically High Angular Resolution Diffusion Imaging (HARDI) [1] of the brain. We want to find robust ways to reveal the architecture of the neural fibers in brain white matter. In Diffusion Tensor Imaging (DTI), the diffusion of water is modeled with a symmetric positive definite second order tensor, based on the assumption that there exists one dominant direction of fibers restricting the thermal motion of water molecules, leading naturally to a Riemannian framework. HARDI may potentially overcome the shortcomings of DTI by allowing multiple relevant directions, but invalidates the Riemannian approach. Instead Finsler geometry provides the natural geometric generalization appropriate for multi-fiber analysis. In this paper we provide the exact criterion to determine whether a field of spherical functions has a Finsler structure. We also show a fiber tracking method in Finsler setting. Our model also incorporates a scale parameter, which is beneficial in view of the noisy nature of the data. We demonstrate our methods on analytic as well as real HARDI data.

1 Introduction

High Angular Resolution Diffusion Imaging (HARDI) is a non-invasive medical imaging modality that measures the attenuation of directional MRI (Magnetic Resonance Imaging) signal due to the diffusion of water molecules. Diffusion weighted measurements are taken in several directions, typically ranging from 50 to 130 (equidistant) angular directions. It is assumed that this diffusion of water molecules reveals relevant information of the underlying tissue architecture. The so-called apparent diffusion coefficient, $D(g)$, is computed from the Stejskal-Tanner [2] formula

$$\frac{S(g)}{S_0} = \exp(-bD(g)), \tag{1}$$

* The Netherlands Organisation for Scientific Research (NWO) is gratefully acknowledged for financial support.

X.-C. Tai et al. (Eds.): SSVM 2009, LNCS 5567, pp. 224–234, 2009.

where $S(g)$ is the signal associated with gradient direction g, S_0 the signal obtained when no diffusion gradient is applied, and b is a parameter associated with the imaging protocol.

In the Diffusion Tensor Imaging framework, (1) is interpreted as

$$\frac{S(g)}{S_0} = \exp(-bg^T Dg) \ , \tag{2}$$

with the 3×3 two-tensor D describing the probability of directional diffusivity at each voxel. A natural way to do geometric analysis on the image, is to use the inverse of the diffusion tensor D as the Riemann metric tensor [3]. This approach has been exploited to some extent in the DTI literature [4], [5], [6], [7]. Since HARDI data typically contains more directional measurements than the traditional DTI, we study it as a metric space, but using a more refined model for directional information than can be accounted for by using only the local position dependent inner product i.e. Riemannian metric. Higher order tensor representations [8], [9], [10], [11] of HARDI data are well suited to differential geometric methods. We mention that Finsler geometry has already been introduced in HARDI setting. In the work of Melonakos et al. [12] the homogeneity condition is forced by normalizing the parameter-vectors, but we take a different approach, using higher order monomial tensors and an ODE-based fiber tracking method.

This paper is organized as follows. In section 2, we give a very short introduction to Finsler geometry and in section 3, we show that indeed HARDI measurements can be modeled with a Finsler-structure and give the specific condition which ensures this. In section 4 we discuss how to switch back and forth between iterative polynomial tensor fitting, that allows Laplace-Beltrami smoothing, and a monomial tensor fitting convenient for constructing a Finsler-norm. In section 5 we show some results of fiber-tracking based on the local Finsler metric and demonstrate it on an analytical example as well as on a real HARDI data of a rat brain scan. In the appendix we will give the details of the construction of the strong convexity criterion.

2 Finsler Geometry

In a perfectly homogeneous and isotropic medium, geometry is Euclidean, and shortest paths are straight lines. In an inhomogeneous space, geometry is Riemannian and the shortest paths are geodesics. If a medium is not only inhomogeneous, but also anisotropic[1], i.e. has innate directional structure, the appropriate geometry is Finslerian [13] [14] and the shortest paths are correspondingly Finsler-geodesics. As a consequence the metric tensor depends on both, position and direction. This is also a natural model for high angular resolution diffusion images.

[1] We will call a medium isotropic if it is endowed with a direction independent inner product, or Riemannian metric. In the literature such a medium is also often referred to as anisotropic due to the directional bias of the metric itself.

Definition 1. *We denote the bundle of tangent spaces $T_{(x,y)}M$ $(y \neq 0)$ as $TM \setminus \{0\}$. A Finsler norm is a function $F : TM \to [0, \infty)$ that satisfies each of the following criteria:*

1. *Differentiability: F is C^∞ on the tangent bundle $TM \setminus \{0\}$.*
2. *Homogeneity: $F(x, \lambda y) = \lambda F(x, y)$.*
3. *Strong convexity: The Hessian matrix, with components*

$$g_{ij}(x, y) = \frac{1}{2} \frac{\partial^2 F^2(x, y)}{\partial y^i \partial y^j}, \tag{3}$$

is positive definite at every point (x, y) of $TM \setminus \{0\}$.

3 Finsler Norm on HARDI Higher Order Tensor Fields

We want to show that higher order tensors, such as those fitted to HARDI data, do define a Finsler norm, which can be used in the analysis of this data. We take as a point of departure a given orientation distribution function (ODF), which if normalized, is a probability density function on the sphere and which can be computed from the data by using one of the methods described in the literature [15], [16], [17], [18], [19]. It models the probability that a given direction corresponds to a direction of a fiber. We use the heuristics that a high probability of finding a fiber in direction y corresponds to a larger diffusivity and at the same time to a shorter travel time from the diffusing particle point of view. Just as in the Riemannian framework, we can actually take our metric tensor to be the inverse of a local ($\mathbf{y}$-dependent) two-tensor. We use the Einstein summation convention $a_i b^i = \sum_i a_i b^i$, and put

$$\mathbf{y} = (\mathbf{y}^1, \mathbf{y}^2, \mathbf{y}^2) = (\sin\theta\cos\varphi, \sin\theta\sin\varphi, \cos\theta) \ , \tag{4}$$

thus $\mathbf{y}$ denotes a unit vector while $y = ||y||\mathbf{y}$ is a general vector in $\mathbb{R}^3$.

We denote the higher order spherical tensor (a homogeneous polynomial restricted to sphere) approximating the ODF as D. As an example, we show how a field of sixth order tensors $D(x)$ defines a Finsler norm. This can be extended directly to all even order tensors.

We put

$$F(x, y) = \left(D_{ijklmn}(x) y^i y^j y^k y^l y^m y^n\right)^{1/6} \ . \tag{5}$$

In the following, we verify the defining criteria stated in Definition 1.

1. Differentiability: The tensor field $D(x)$ is constructed by fitting a tensor to the set of angular samples at each voxel, using a least squares method. The data set with fixed angle is continuous in x by linear interpolation between the sample points and differentiable w.r.t. x using Gaussian derivatives. Therefore the tensor field itself is differentiable in x, and because D is always positive, differentiability of F w.r.t. x follows. The differentiability of F in y is obvious from Eq. (5).

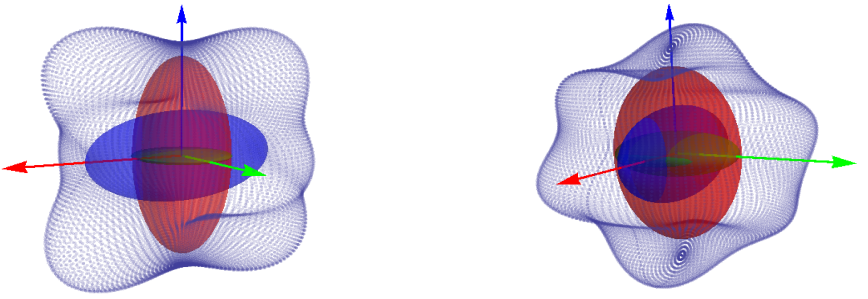

Fig. 1. Left:A fourth order spherical harmonic (or tensor), representing the (not convexified) norm function and 3 ellipsoids illustrating the metric tensors corresponding to the 3 vectors with same color. Right: Similarly a sixth order spherical harmonic function with 3 metric tensors.

2. Homogeneity: Indeed for any $\alpha \in \mathbb{R}_+$, $x \in M$, $v \in T_xM$:

$$F(x, \alpha v) = \left(D_{ijklmn}(x)\alpha v^i \alpha v^j \alpha v^k \alpha v^l \alpha v^m \alpha v^n\right)^{1/6} = \alpha F(x, v) \ . \quad (6)$$

3. Strong convexity:
We now state a strong convexity criterion for a general Finsler norm in $\mathbb{R}^3$, by analogy to the $\mathbb{R}^2$-criterion by Bao et al [13]. We have put the derivation of the condition into the appendix, and merely state the result here. We consider the so-called indicatrix of the norm function F at any fixed x, which is the set $\{g \mid g : (\theta, \varphi) \to \mathbb{R}^3 \ , \ F(g) = 1\}$. In our case the indicatrix is the ODF, which can be easily seen from the homogeneity condition 2. in Definition 1.

$$F(\mathbf{y}(\theta, \varphi)) = \frac{1}{ODF(\theta, \varphi)} \implies F(ODF(\theta, \varphi) \cdot \mathbf{y}(\theta, \varphi)) = 1 \ .$$

We denote $\dot{g}_\theta := \frac{\partial}{\partial \theta}(g)$, $\ddot{g}_\theta := \frac{\partial^2}{\partial \theta^2}(g)$ and similarly for φ. We define the following three matrices:

$$m = \begin{pmatrix} g^1 & g^2 & g^3 \\ \dot{g}^1_\theta & \dot{g}^2_\theta & \dot{g}^3_\theta \\ \dot{g}^1_\varphi & \dot{g}^2_\varphi & \dot{g}^3_\varphi \end{pmatrix} \ , \ m_\theta = \begin{pmatrix} \ddot{g}^1_\theta & \ddot{g}^2_\theta & \ddot{g}^3_\theta \\ \dot{g}^1_\theta & \dot{g}^2_\theta & \dot{g}^3_\theta \\ \dot{g}^1_\varphi & \dot{g}^2_\varphi & \dot{g}^3_\varphi \end{pmatrix} \ , \ m_\varphi = \begin{pmatrix} \ddot{g}^1_\varphi & \ddot{g}^2_\varphi & \ddot{g}^3_\varphi \\ \dot{g}^1_\theta & \dot{g}^2_\theta & \dot{g}^3_\theta \\ \dot{g}^1_\varphi & \dot{g}^2_\varphi & \dot{g}^3_\varphi \end{pmatrix} \ . \quad (7)$$

Then the strong convexity requires:

$$\frac{\det(m_\theta)}{\det(m)} > 0 \ , \quad \text{and} \quad \frac{\det(m_\varphi)}{\det(m)} > \frac{(g_{ij}\dot{y}^i_\theta \dot{y}^j_\varphi)^2}{g_{ij}\dot{y}^i_\theta \dot{y}^j_\theta} \ . \quad (8)$$

Since we use linear interpolation between tensors, we only need to check the condition at original data-points. This condition is always met in our ODF-data, and we expect it to hold quite generally.

The goal of this section was to define a Finsler-structure and in particular a Finsler **metric tensor** $g_{ij}(x, y)$ corresponding to a given tensorial ODF. Indeed

in case the ODF is a symmetric tensor of order two, this metric tensor is equivalent to the Riemann metric tensor. Following our Finsler approach, instead of one metric tensor per voxel we obtain a bundle of metric tensors at any x. For illustration, see Fig.1.

4 Transforming a Polynomial Tensor to a Monomial Tensor

Assume we wish to apply Laplace-Beltrami smoothing to our spherical data, by which we obtain a field of spherical functions at any desired scale, and that we wish to use a tensorial representation of the data instead of spherical harmonics. As is shown in [10], this smoothing is easy to do, using iterative polynomial tensor fitting. The point here is that for Finsler analysis, we would rather work with a tensor representation of monomial form

$$D(y) = D_{i_1 \cdots i_n} \mathbf{y}^{i_1} \cdots \mathbf{y}^{i_n} \ , \tag{9}$$

than with the equivalent polynomial expression

$$\tilde{D}(y) = \sum_{k=0}^{n} \tilde{D}_{i_1 \cdots i_k} \mathbf{y}^{i_1} \cdots \mathbf{y}^{i_k} \ , \tag{10}$$

but still exploit the convenient (co-domain) scale space representation of the latter:

$$\tilde{D}(y, \tau) = \sum_{k=0}^{n} e^{-\tau k(k+1)} \tilde{D}_{i_1 \cdots i_k} \mathbf{y}^{i_1} \cdots \mathbf{y}^{i_k} \ . \tag{11}$$

This poses no problem, since we can rather easily transform the polynomial expression to a monomial one, using the fact that our polynomials are restricted to the sphere (eq. (4)), thus we may expand a lower order tensor to a sparse higher order one and symmetrize it. We can also always transform the monomial expression to polynomial sum of irreducible monomial tensors using Clebsch-projection [20].

5 Fiber Tracking in HARDI Data Using Finsler Geometry

In DTI setting the most straightforward way of tracking fibers is to follow the principal eigenvector corresponding to the largest eigenvalue of the diffusion tensor until some stopping criterion. This method cannot reveal crossings and only provides a single direction (if at all) per voxel. Instead computing the shortest paths according to the diffusion-induced Riemann metric tensor, we could expect these to be the candidates for real fibers [5]. Of course, most of the shortest paths (geodesics) are not representing actual fibers, and therefore we should extract the potential neural fibers from arbitrary geodesics based on their connectivity [6]. We show some results of solving well-connected geodesics in an analytic as well as in a real rat brain data.

5.1 Analytic Tensor Field

We treat an analytic norm field in $\mathbb{R}^2$, but the situation can be directly extended to $\mathbb{R}^3$. Let us take as a convex norm function at each spatial position

$$F(\varphi) = (\cos 4\varphi + 4)^{\frac{1}{4}} = \left(5\cos^4\varphi + 2\cos^2\varphi\sin^2\varphi + 5\sin^4\varphi\right)^{\frac{1}{4}} \ . \tag{12}$$

This is an example of fourth order tensor on unit vectors. Such a tensor field could represent an infinitely dense field of orthogonally crossing fibers. From the fact that F has no x-dependence we conclude that the geodesic coefficients vanish and that the geodesics coincide with the Euclidean geodesics $\gamma(t) = (t \cdot \cos\varphi, t \cdot \sin\varphi)$, i.e. straight lines. However the so-called connectivity of a geodesic [6], [21] is relatively large, only in cases, where the directional norm function is correspondingly small. In Finsler setting the connectivity measure $m(\gamma)$ is:

$$m(\gamma) = \frac{\int \sqrt{\eta_{ij}\dot{\gamma}^i\dot{\gamma}^j}dt}{\int \sqrt{g_{ij}(\gamma,\dot{\gamma})\dot{\gamma}^i\dot{\gamma}^j}dt} \ , \tag{13}$$

where the $\eta_{ij}(\gamma)$ represents the covariant Euclidean metric tensor which in Cartesian coordinates reduces to the constant identity matrix, $\dot{\gamma}$ the tangent to the curve γ and $g_{ij}(\gamma,\dot{\gamma})$ the Finsler-metric tensor (which depends not only on the position on the curve but also on the tangent of the curve). For illustration we compute explicitly the metric tensors, using Cartesian coordinates:

$$g_{ij} = \frac{1}{(5\cos\varphi^4 + 2\cos\varphi^2\sin\varphi^2 + 5\sin\varphi^4)^{3/2}} \begin{pmatrix} g_{11} & g_{12} \\ g_{21} & g_{22} \end{pmatrix} \ , \tag{14}$$

where

$$\begin{aligned} g_{11} &= 5(5\cos\varphi^6 + 3\cos\varphi^4\sin\varphi^2 + 15\cos\varphi^2\sin\varphi^4 + \sin\varphi^6) \\ g_{12} &= g_{21} = -48\cos\varphi^3\sin\varphi^3 \\ g_{22} &= 5(\cos\varphi^6 + 15\cos\varphi^4\sin\varphi^2 + 3\cos\varphi^2\sin\varphi^4 + 5\sin\varphi^6) \end{aligned}$$

The strong convexity criterion $\frac{\ddot{g}^1\dot{g}^2 - \dot{g}^1\ddot{g}^2}{\dot{g}^1 g^2 - g^1\dot{g}^2} > 0$ in $\mathbb{R}^2$ [13] on the indicatrix $g(\varphi)$, for metric (14) is satisfied for every φ, since

$$\frac{\ddot{g}^1\dot{g}^2 - \dot{g}^1\ddot{g}^2}{\dot{g}^1 g^2 - g^1\dot{g}^2} = \frac{13 - 8\cos 4\varphi}{(4 + \cos 4\varphi)^2} > 0 \ . \tag{15}$$

The connectivity measure for a (Euclidean) geodesic γ can be computed analytically:

$$m(\gamma) = \frac{\int dt}{\int (4 + \cos(4\varphi))^{1/4} dt} \ , \tag{16}$$

which gives the maximal connectivities in directions $\{\frac{\pi}{4}, \frac{3\pi}{4}, \frac{5\pi}{4}, \frac{7\pi}{4}\}$, as expected. See Fig. 2 for an illustration. We observe that on such a norm field the Riemannian (DTI) framework would result in Euclidean geodesics and constant connectivity over all geodesics thus revealing no information at all of the angular heterogeneity.

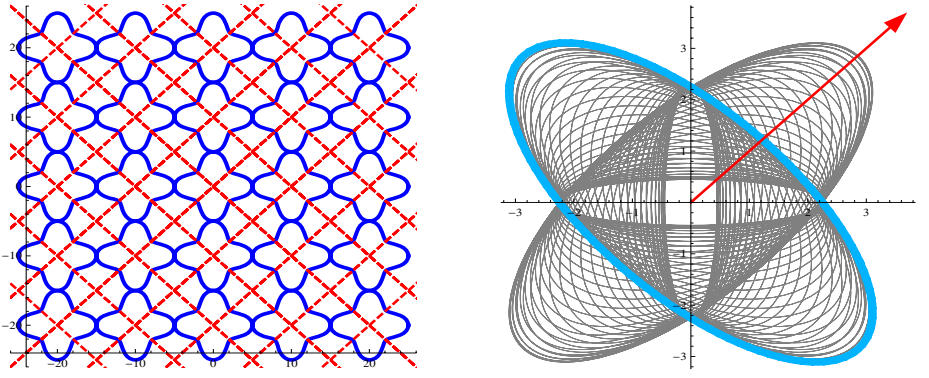

Fig. 2. Left:A field of fourth order spherical harmonics as in the norm function eq. (12) representing dense crossings and some well connected geodesics, colored in red. Right: 200 equiangular metric tensors of the same norm function, and an ellipse with light blue color corresponding to the metric in direction $\varphi = \frac{\pi}{4}$.

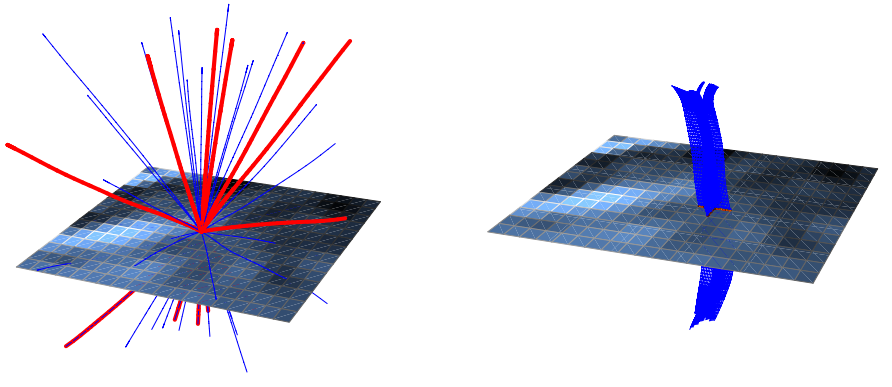

Fig. 3. Left:Finsler geodesics emanating from a voxel, and the most connective ones in red. Right: Fibers through same neighborhood in the traditional DTI principal eigenvector tracking.

5.2 Real Rat Brain Data

The Subthalamic Nucleus is a small area in the brain, that is involved in physiopathology of Parkinson's disease [22]. We computed the Finsler geodesics and their connectivities, having an initial point in several central voxels in the Subthalamic Nucleus. These voxels were located based on comparison to an atlas of rat brain [23]. We tracked Finsler geodesics using the standard equation (ODE-formulation) [14](p.78) and second order Taylor approximation, with initial directions as the 49 measurement directions, stepsize 0.2 voxel size and for 10 steps. Then we selected those 30% of all geodesics that have the best connectivity. Compared to the traditional DTI-tracking, we found that one of the main

directions with strong connectivity typically coincide with the DTI-fibers, but we also found other potential fiber directions. For illustration see Fig. 3.

6 Conclusions and Future Work

We have seen that it is indeed possible to analyze spherical tensor fields using Finsler geometry. It gives new methods to work with the data and also has the potential to give new information on the data. Finsler geodesics and Finsler curvatures are examples of geometric measures that can be applied on HARDI fiber-analysis, and which will be a subject of extensive future work.

Acknowledgement

The rat brain data acquired for a study [24], was kindly provided by Ellen Brunenberg.

References

1. Tuch, D., Reese, T., Wiegell, M., Makris, N., Belliveau, J., van Wedeen, J.: High angular resolution diffusion imaging reveals intravoxel white matter fiber heterogeneity. Magnetic Resonance in Medicine 48(6), 1358–1372 (2002)
2. Stejskal, E., Tanner, J.: Spin diffusion measurements: Spin echoes ion the presence of a time-dependent field gradient. The Journal of Chemical Physics 42(1), 288–292 (1965)
3. Cohen de Lara, M.: Geometric and symmetry properties of a nondegenerate diffusion process. The Annals of Probability 23(4), 1557–1604 (1995)
4. O'Donnell, L., Haker, S., Westin, C.F.: New approaches to estimation of white matter connectivity in diffusion tensor MRI: Elliptic PDEs and geodesics in a tensor-warped space. In: Dohi, T., Kikinis, R. (eds.) MICCAI 2002. LNCS, vol. 2488, pp. 459–466. Springer, Heidelberg (2002)
5. Lenglet, C., Deriche, R., Faugeras, O.: Inferring white matter geometry from diffusion tensor MRI: Application to connectivity mapping. In: Pajdla, T., Matas, J.G. (eds.) ECCV 2004. LNCS, vol. 3024, pp. 127–140. Springer, Heidelberg (2004)
6. Astola, L., Florack, L., ter Haar Romeny, B.: Measures for pathway analysis in brain white matter using diffusion tensor images. In: Karssemeijer, N., Lelieveldt, B. (eds.) IPMI 2007. LNCS, vol. 4584, pp. 642–649. Springer, Heidelberg (2007)
7. Astola, L., Florack, L.: Sticky vector fields and other geometric measures on diffusion tensor images. In: MMBIA 2008, IEEE Computer Society Workshop on Mathematical Methods in Biomedical Image Analysis, held in conjunction with CVPR 2008, Anchorage, Alaska, The United States. CVPR, vol. 20, pp. 1–7. Springer, Heidelberg (2008)
8. Özarslan, E., Mareci, T.: Generalized diffusion tensor imaging and analytical relationships between diffusion tensor imaging and high angular resolution diffusion imaging. Magnetic resonance in Medicine 50, 955–965 (2003)
9. Barmpoutis, A., Jian, B., Vemuri, B., Shepherd, T.: Symmetric positive 4^{th} order tensors and their estimation from diffusion weighted MRI. In: Karssemeijer, N., Lelieveldt, B. (eds.) IPMI 2007. LNCS, vol. 4584, pp. 308–319. Springer, Heidelberg (2007)

10. Florack, L., Balmashnova, E.: Decomposition of high angular resolution diffusion images into a sum of self-similar polynomials on the sphere. In: Proceedings of the Eighteenth International Conference on Computer Graphics and Vision, GraphiCon 2008, Moscow, Russian Federation, June 2008, pp. 26–31 (2008) (invited paper)
11. Florack, L., Balmashnova, E.: Two canonical representations for regularized high angular resolution diffusion imaging. In: MICCAI Workshop on Computational Diffusion MRI, New York, USA, September 10, 2008, pp. 94–105 (2008)
12. Melonakos, J., Pichon, E., Angenent, S., Tannenbaum, A.: Finsler active contours. IEEE Transactions on Pattern Analysis and Machine Intelligence 30(3), 412–423 (2008)
13. Bao, D., Chern, S.S., Shen, Z.: An Introduction to Riemann-Finsler Geometry. Springer, Heidelberg (2000)
14. Shen, Z.: Lectures on Finsler Geometry. World Scientific, Singapore (2001)
15. Tuch, D.: Q-ball imaging. Magnetic Resonance in Medicine 52(4), 577–582 (2002)
16. Jansons, K., Alexander, D.: Persistent angular structure: New insights from diffusion magnetic resonance imaging data. Inverse Problems 19, 1031–1046 (2003)
17. Özarslan, E., Shepherd, T., Vemuri, B., Blackband, S., Mareci, T.: Resolution of complex tissue microarchitecture using the diffusion orientation transform. NeuroImage 31, 1086–1103 (2006)
18. Jian, B., Vemuri, B., Özarslan, E., Carney, P., Mareci, T.: A novel tensor distribution model for the diffusion-weighted MR signal. NeuroImage 37, 164–176 (2007)
19. Descoteaux, M., Angelino, E., Fitzgibbons, S., Deriche, R.: Regularized, fast and robust analytical q-ball imaging. Magnetic Resonance in Medicine 58(3), 497–510 (2006)
20. Müller, C. (ed.): Analysis of Spherical Symmetries in Euclidean Spaces. Applied Mathematical Sciences, vol. 129. Springer, New York (1998)
21. Prados, E., Soatto, S., Lenglet, C., Pons, J.P., Wotawa, N., Deriche, R., Faugeras, O.: Control Theory and Fast Marching Techniques for Brain Connectivity Mapping. In: Proceedings of the IEEE computer society conference on computer vision and pattern recognition, New York, USA, vol. 1, pp. 1076–1083. IEEE Computer Society Press, Los Alamitos (2006)
22. Hamani, C., Saint-Cyr, J., Fraser, J., Kaplitt, M., Lozano, A.: The subthalamic nucleus in the context of movement disorders. Brain, a Journal of Neurology 127, 4–20 (2004)
23. Paxinos, G., Watson, C.: The Rat Brain In Stereotaxic Coordinates. Academic Press, San Diego (1998)
24. Brunenberg, E., Prckovska, V., Platel, B., Strijkers, G., ter Haar Romeny, B.M.: Untangling a fiber bundle knot: Preliminary results on STN connectivity using DTI and HARDI on rat brains. In: Proceedings of the 17th Meeting of the International Society for Magnetic Resonance in Medicine (ISMRM), Honolulu, Hawaii (2009)

Appendix

We seek the general condition for

$$g_{ij}(y)v^i v^j > 0 \ , \tag{17}$$

to be valid in $\mathbb{R}^3 (= T_x M)$. From the homogeneity of the norm function F, it follows that it is sufficient to have this condition on the unit level set of the norm. We consider this level surface i.e. the set of vectors y for which $F(y) = 1$ and a parametrization $y(\theta, \varphi) = (y^1(\theta, \varphi), y^2(\theta, \varphi), y^3(\theta, \varphi))$. In what follows we abbreviate $g_{ij} = g_{ij}(x, y)$. From $F(y) = 1$ we have

$$g_{ij} y^i y^j = 1 \ . \tag{18}$$

Taking derivatives of both sides and using a consequence of Euler's theorem for homogeneous functions ([13] p.5) that says

$$\frac{\partial g_{ij}}{\partial y^k} y^k = 0 \ , \tag{19}$$

we obtain

$$\begin{aligned} g_{ij} \dot{y}^i_\theta y^j &= 0 \\ g_{ij} \dot{y}^i_\varphi y^j &= 0 \ , \end{aligned} \tag{20}$$

implying $\dot{y}_\theta \perp_g y$ and $\dot{y}_\varphi \perp_g y$.

Taking derivatives once more, we get

$$\begin{aligned} g_{ij} \ddot{y}^i_\theta y^j &= -g_{ij} \dot{y}^i_\theta \dot{y}^j_\theta \\ g_{ij} \ddot{y}^i_\varphi y^j &= -g_{ij} \dot{y}^i_\varphi \dot{y}^j_\varphi \\ g_{ij} \ddot{y}^i_{\theta\varphi} y^j &= -g_{ij} \dot{y}^i_\theta \dot{y}^j_\varphi \ . \end{aligned} \tag{21}$$

We may express an arbitrary vector v as a linear combination of orthogonal basis vectors:

$$v = \alpha y + \beta \dot{y}_\theta + \gamma \left(\dot{y}_\varphi - \frac{\langle \dot{y}_\varphi, \dot{y}_\theta \rangle}{\langle \dot{y}_\theta, \dot{y}_\theta \rangle} \dot{y}_\theta \right) . \tag{22}$$

We substitute this expression for v to the left hand side of (17) and obtain:

$$g_{ij} v^i v^j = \alpha^2 g_{ij} y^i y^j + \beta^2 g_{ij} \ddot{y}^i_\theta y^j + \gamma^2 \left(g_{ij} \ddot{y}^i_\varphi y^j - \frac{(g_{ij} \dot{y}^i_\theta \dot{y}^j_\varphi)^2}{g_{ij} \dot{y}^i_\theta \dot{y}^j_\theta} \right) \ , \tag{23}$$

because the mixed terms vanish due to the orthogonality of basis vectors.

On the other hand, for y's on the indicatrix we have as a consequence of Euler's theorem on homogeneous functions (denoting $F_{y^i} = \frac{\partial F}{\partial y^i}$):

$$F_{y^i} y^i = F(y) = 1 \ . \tag{24}$$

Differentiating eq. (24) w.r.t. θ and φ, we obtain two equations:

$$F_{y^i}\dot{y}^i_\theta = 0 \tag{25}$$
$$F_{y^i}\dot{y}^i_\varphi = 0\ , \tag{26}$$

for F is a homogeneous function.

The matrices m, m_θ, m_φ are as defined in eq. (7). Solving system of equations (24), (25) and (25) we get:

$$F_{y^1} = \frac{\dot{y}^2_\varphi \dot{y}^3_\theta - \dot{y}^3_\varphi \dot{y}^2_\theta}{\det(m)}\ , F_{y^2} = \frac{\dot{y}^3_\varphi \dot{y}^1_\theta - \dot{y}^1_\varphi \dot{y}^3_\theta}{\det(m)}\ , F_{y^3} = \frac{\dot{y}^1_\varphi \dot{y}^2_\theta - \dot{y}^2_\varphi \dot{y}^1_\theta}{\det(m)}\ . \tag{27}$$

Now using equalities

$$F_{y^i} = g_{ij}y^j, \qquad g_{ij}\ddot{y}^i{}_\theta y^j = F_{y^k}\ddot{y}^k_\theta, \qquad g_{ij}\ddot{y}^i{}_\varphi y^j = F_{y^k}\ddot{y}^k_\varphi\ , \tag{28}$$

and

$$-g_{ij}\ddot{y}^i_\theta y^j = \frac{\det(m_\theta)}{\det(m)}\ , \qquad -g_{ij}\ddot{y}^i_\varphi y^j = \frac{\det(m_\varphi)}{\det(m)} \tag{29}$$

we obtain

$$g_{ij}v^iv^j = \alpha^2 - \beta^2 g_{ij}\ddot{y}^i_\theta y^j - \gamma^2\left(g_{ij}\ddot{y}^i_\varphi y^j - \frac{(g_{ij}\dot{y}^i_\theta \dot{y}^j_\varphi)^2}{g_{ij}\dot{y}^i_\theta \dot{y}^j_\theta}\right) > 0 \tag{30}$$

if

$$\frac{\det(m_\theta)}{\det(m)} > 0 \qquad \text{and} \qquad \frac{\det(m_\varphi)}{\det(m)} > \frac{(g_{ij}\dot{y}^i_\theta \dot{y}^j_\varphi)^2}{g_{ij}\dot{y}^i_\theta \dot{y}^j_\theta}\ . \tag{31}$$